iScience

CellPress
OPEN ACCESS

Article

Mea6/cTAGE5 cooperates with TRAPPC12 to regulate PTN secretion and white matter development

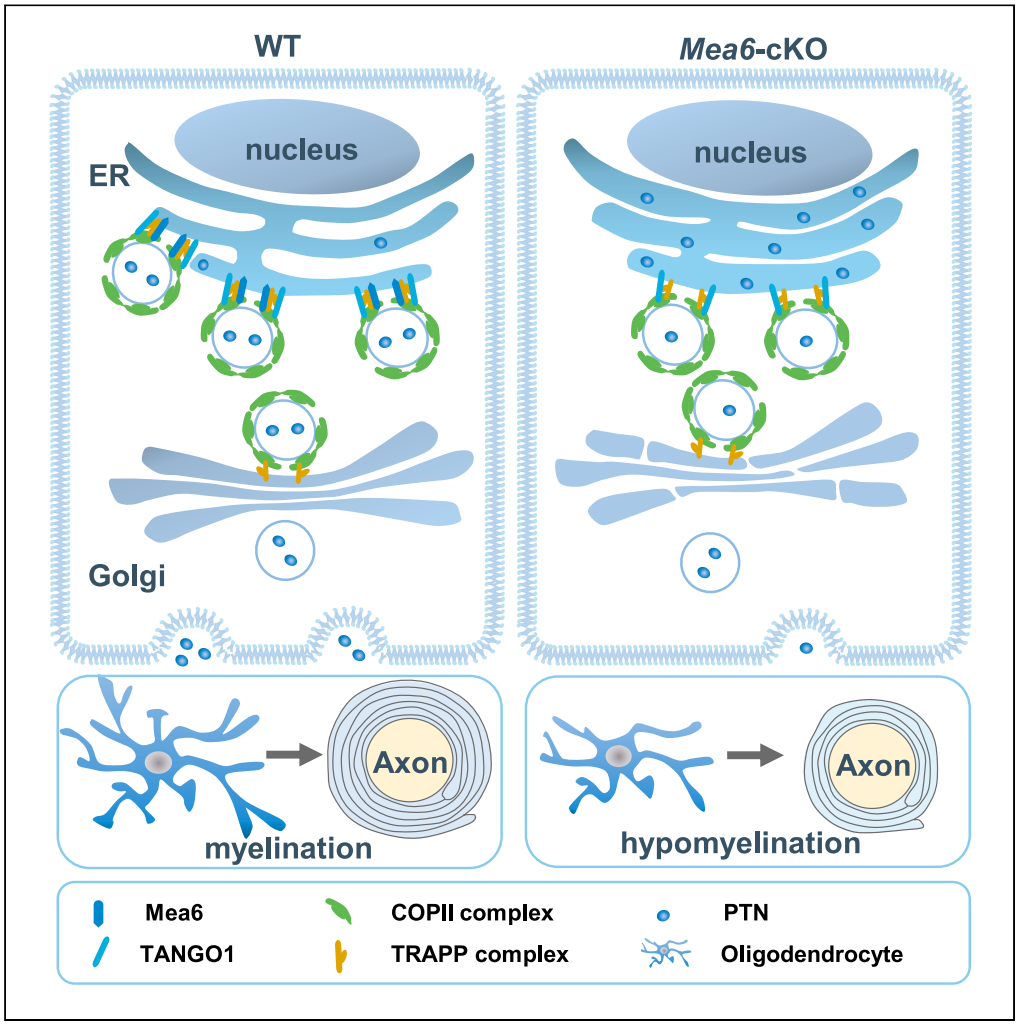

Tiantian Ma, Yaqing Wang, Laikang Yu, ..., Kangmin He, Li Zhao, Zhiheng Xu

matiantian@ustc.edu.cn (T.M.)
zhxu@genetics.ac.cn (Z.X.)

Highlights

TRAPPC12 interacts with Mea6 and COPII components at ER exit site

TRAPPC12 and MEA6 regulate oligodendrocyte progenitor cell (OPC) development

Mea6 cKO in OPC leads to hypomyelination, abnormal synaptic function and behaviors

Mea6 cKO affects pleiotrophin (PTN) secretion and PTN improves OPC development

Ma et al., iScience *27*, 109180
March 15, 2024
https://doi.org/10.1016/j.isci.2024.109180

iScience

CellPress
OPEN ACCESS

Article

Mea6/cTAGE5 cooperates with TRAPPC12 to regulate PTN secretion and white matter development

Tiantian Ma,[1,2,4,*] Yaqing Wang,[1,2,4] Laikang Yu,[3] Jinghua Liu,[1,2] Tao Wang,[1] Pengyu Sun,[1,2] Yinghang Feng,[1,2] Dan Zhang,[1,2] Lei Shi,[1] Kangmin He,[1,2] Li Zhao,[3] and Zhiheng Xu[1,2,5,*]

SUMMARY

Mutations of TRAPPC12 are associated with progressive childhood encephalopathy including abnormal white matter. However, the underlying pathogenesis is still unclear. Here, we found that *Trappc12* deficiency in CG4 and oligodendrocyte progenitor cells (OPCs) affects their differentiation and maturation. In addition, TRAPPC12 interacts with Mea6/cTAGE5, and *Mea6/cTAGE5* ablation in OPCs affects their proliferation and differentiation, leading to marked hypomyelination, compromised synaptic functionality, and aberrant behaviors in mice. We reveal that TRAPPC12 is associated with COPII components at ER exit site, and *Mea6/cTAGE5* cKO disrupts the trafficking pathway by affecting the distribution and/or expression of TRAPPC12, SEC13, SEC31A, and SAR1. Moreover, we observed marked disturbances in the secretion of pleiotrophin (PTN) in *Mea6*-deficient OPCs. Notably, exogenous PTN supplementation ameliorated the differentiation deficits of these OPCs. Collectively, our findings indicate that the association between TRAPPC12 and MEA6 is important for cargo trafficking and white matter development.

INTRODUCTION

Governed by intricate signaling pathways, oligodendrocyte progenitor cells (OPCs) undergo proliferation and differentiation, culminating in the formation of lipid-dense membranous structures called myelin sheaths, which envelop neuronal axons to expedite accurate and efficient action potential transmission.[1,2] Furthermore, emerging evidence substantiates the notion that oligodendrocytes (OLs) supply axons with nutritional sustenance and facilitate signal transduction.[3,4] Hypomyelination or demyelination, attributable to a myriad of etiologies, ultimately triggers axonal degeneration, inflammatory responses or behavior change.[5,6] The consequent clinical manifestations, encompassing motor dysfunction, cognitive deficits, and social abnormalities, severely undermine patients' quality of life.[7,8] However, due to the convoluted and multifaceted origins of myelin sheath aberrations, devising symptomatic treatments is still challenging. As such, exploring deeply into the mechanisms governing myelination and the pathogenesis of associated disorders is imperative.

During oligodendrocyte differentiation, their surfaces undergo a marked expansion within a brief temporal window, indicating that this process requires the synthesis and transport of abundant proteins and lipids. Coat protein complex II (COPII) orchestrates the trafficking of the majority of proteins and lipids from the endoplasmic reticulum (ER) to downstream destinations, including the ER-Golgi intermediate compartment (ERGIC), Golgi apparatus, and other organelles.[9–11]

Different transport protein particle[12] complexes function after the assembly and fission of COPII vesicles from ER exit site (ERES) and mediate the intra-Golgi traffic and Golgi exit.[13,14] Mutations in components of TRAPP complex, TRAPPC12 and TRAPPC9, have been reported to cause progressive childhood encephalopathy including dysplasia of white matter in patients.[15–17]

Mea6 (meningioma-expressed antigen 6), also named cTAGE5 (cutaneous T cell lymphoma-associated antigen 5C), is indispensable for the initial assembly of the COPII complex.[9,18,19] Previous studies demonstrated that eliminating *Mea6* from the brain causes severe defects in brain development, including a thinner corpus callosum, and establishes Mea6 as vital for white matter formation and myelin sheath lipid component maintenance.[19,20] However, whether and how Mea6/cTAGE5 regulates different stages of OL development and myelination, and the underlying mechanisms remain elusive.

In this study, we found that knockout or knockdown of *Trappc12* resulted in reduced differentiation capacity of CG4 cells and OPCs. TRAPPC12 interacted with Mea6 and SEC31A, and deletion of *Trappc12* led to dispersed distribution of SEC13/SEC31. Furthermore, mice with OL-specific deletion of *Mea6* exhibited pronounced hypomyelination and aberrant behaviors. Dysregulated expression of TRAPPC12, SEC31, SEC13, and SAR1-GTP was detected in the corpus callosum of *Mea6* cKO mice. Importantly, significant retention of PTN was observed in *Mea6*-deficiency OPCs and PTN supplement partially rescued their defect in differentiation.

[1]State Key Laboratory of Molecular Developmental Biology, Institute of Genetics and Developmental Biology, Chinese Academy of Sciences, Beijing 100101, China
[2]University of Chinese Academy of Sciences, Beijing 100083, China
[3]Key Laboratory of Physical Fitness and Exercise, Ministry of Education, Beijing Sport University, Beijing, Haidian District, China
[4]These authors contributed equally
[5]Lead contact
*Correspondence: matiantian@ustc.edu.cn (T.M.), zhxu@genetics.ac.cn (Z.X.)
https://doi.org/10.1016/j.isci.2024.109180

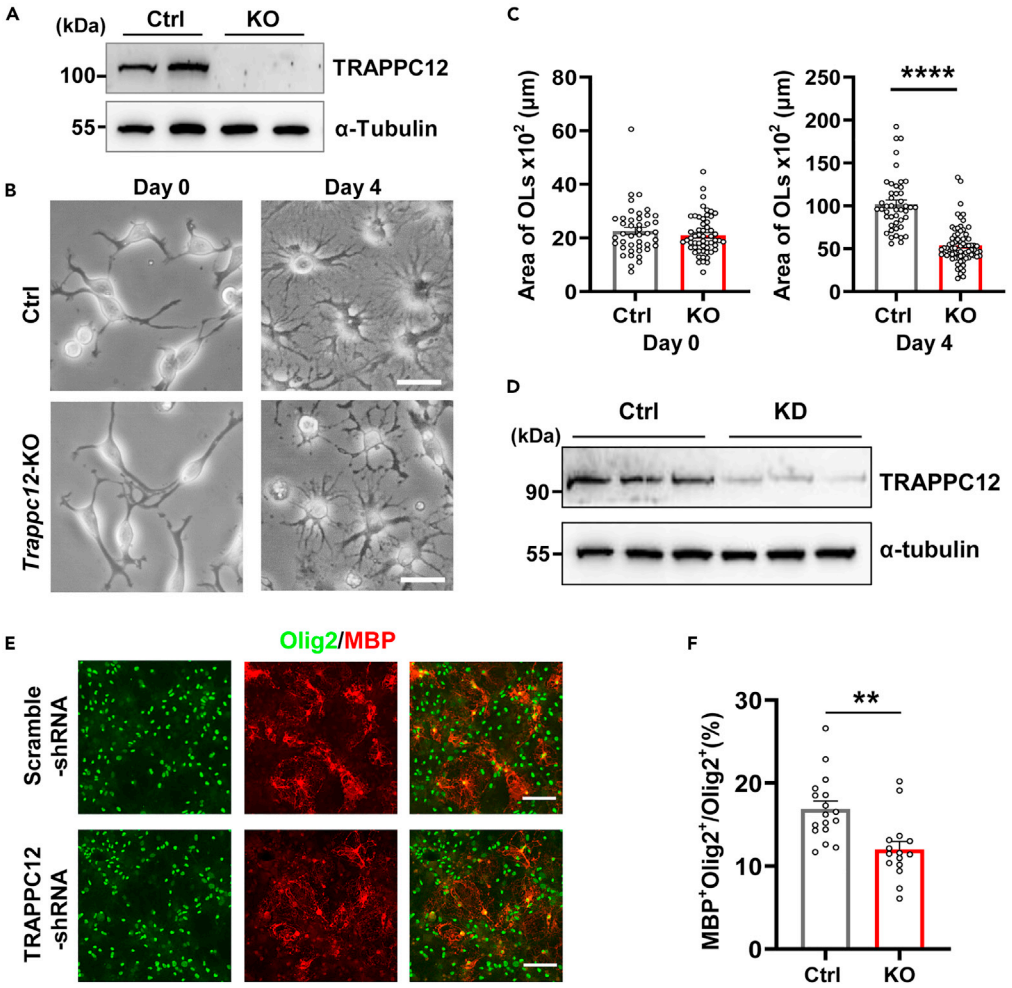

Figure 1. *Trappc12* KO affects CG4 cell and OPCs differentiation

(A) *Trappc12* knockout in CG4 cells was confirmed by immunoblot. Samples were from different single clones.

(B) Images of CG4 cell morphology during differentiation (Days 0 and 4). Scale bars: 50 μm.

(C) Quantification of cell area from (B) (n = 3 independent single clones in each group).

(D) shRNA knockdown efficiency of lentivirus expressing scramble or shRNA for Trappc12 in OPCs.

(E) Immunostaining of Olig2 and MBP in cultured OLs infected with lentivirus expressing scramble or shRNA for Trappc12 at 6 days after differentiation. Scale bar: 100 μm.

(F) Quantification of MBP^+ cells over $Olig2^+$ cells (n = 4 in each group). Data represent the mean ± SEM. **p < 0.01, ****p < 0.0001, Two-tailed unpaired Student's *t* test.

RESULTS

TRAPPC12 is required for CG4 and OPC differentiation

Mutations of TRAPPC12, a component of the TRAPPIII complex functioning in the ER-to-Golgi transportation, are associated with defects in the development of white matter.[16,17] To determine whether TRAPPC12 plays a role in oligodendrocyte development, we eliminated *Trappc12* from CG4 cells (an oligodendrocyte progenitor cell line) using CRISPR Cas9 technology (Figure 1A). The cell complexity was significantly decreased in *Trappc12*-KO cells 4 days after differentiation (Figures 1B and 1C). We also used shRNA packaged in lentivirus to knock down Trappc12 expression in primary cultured mouse OPCs (Figure 1D). The percentage of MBP^+ cells was significantly lower in the knockdown group after 6 days of differentiation (Figures 1E and 1F). These results indicate that TRAPPC12 is important for OPC differentiation and support the genetic evidence that TRAPPC12 mutation contributes to the dysplasia of white matter in patients.

TRAPPC12 expression in ERES and interaction with Mea6

Because TRAPPC12 is involved in the assembly of COPII outer layer and our previous proteomic results implicated that Trappc12 expression might be downregulated in *Mea6* $^{fl/fl}$; *Nestin-Cre* cortical brain,[19,21] we therefore inspected the expression of Trappc12 in cultured OPCs and

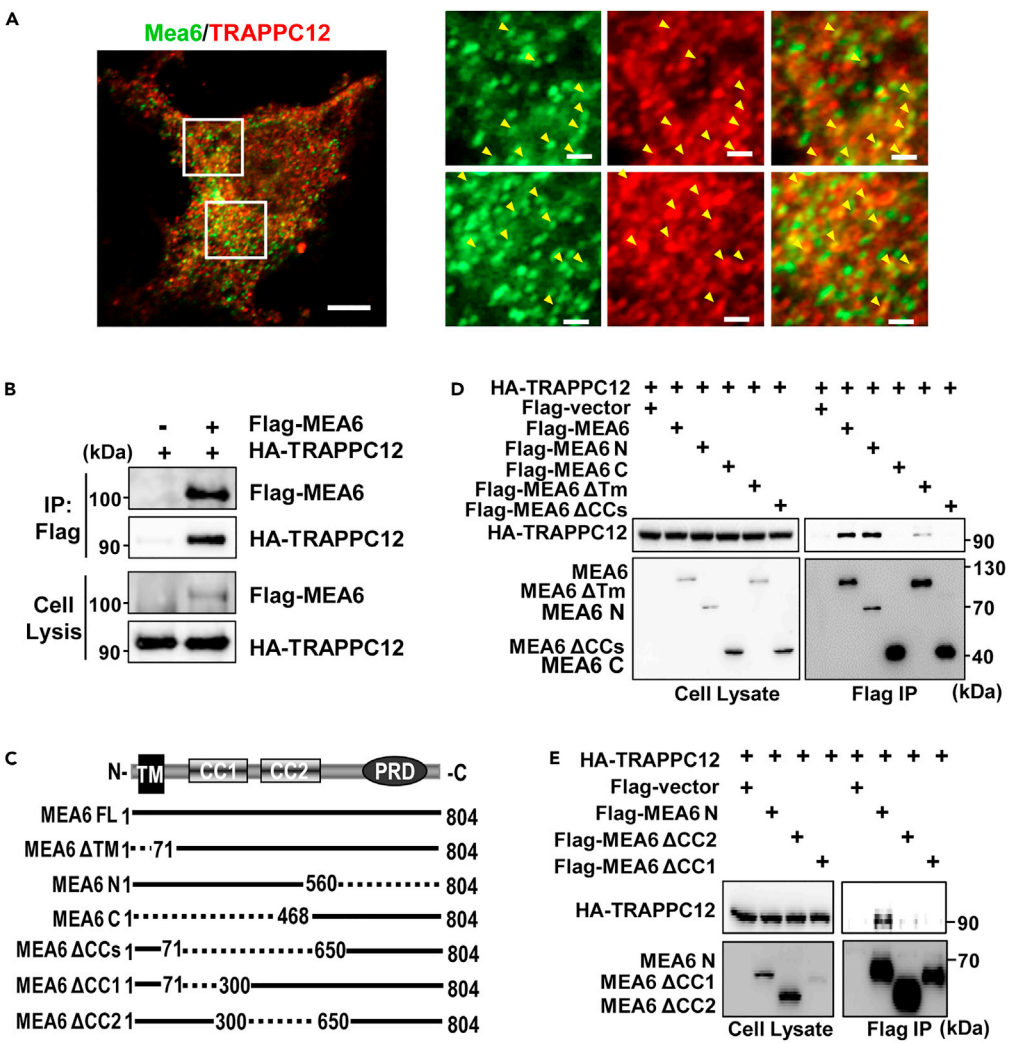

Figure 2. TRAPPC12 interacts with MEA6

(A) Representative images of immunostaining showing partial co-localization of MEA6 and TRAPPC12 in cultured mouse OPCs. Inset figures are magnified images. Scale bars: 5 μm, insets: 1 μm.

(B) TRAPPC12 interacts with MEA6. Flag-MEA6 was transfected into HEK293 cells either alone or together with HA-TRAPPC12. Co-IP was performed in cell lysates with Flag beads.

(C) Schematic representation of the MEA6 full-length or different deletion mutants. TM: transmembrane domain; CC: coiled-coil domain; PRD: proline-rich domain.

(D and E) Interaction between TRAPPC12 and full-length MEA6 or mutants were analyzed by Co-IP. Different Flag-MEA6 constructs or vector was co-transfected with HA-TRAPPC12 in HEK293 cells. Co-IP was performed in cell lysates with Flag beads.

found that it partially colocalized with Mea6 (Figure 2A). In CG4 cells transfected with the COPII components SEC24C and SEC31A, TRAPPC12 was markedly accumulated at SEC-positive puncta (Figure S1A). We confirmed that TRAPPC12 could interact with the outer components of COPII SEC31A, as reported.[21] However, TRAPPC12 was likely to interact with SEC13A only in the presence of SEC31 (Figure S1B).

The colocalization of TRAPPC12 with MEA6 and COPII components indicates the location of TRAPPC12 in ERES. We, therefore, explored whether TRAPPC12 interacts with MEA6. Constructs encoding TRAPPC12 and MEA6 were transfected into 293 cells either alone or in combination, and co-immunoprecipitation (Co-IP) assay revealed that TRAPPC12 interacted with MEA6 (Figure 2B). We went on to dissect which domain of MEA6 was required for its interaction with TRAPPC12. We generated different deletion mutants of MEA6 (Figure 2C) and they were transfected into 293 cells either alone or in combination. Co-IP experiments revealed that the two coil-coil domains of MEA6 were essential for the interaction between MEA6 and TRAPPC12 (Figure 2D). We further dissected the coil-coil domains into coil-coil 1 and coil-coil 2 domains and found out both two coil-coils domain were important for MEA6 to interact with TRAPPC12 (Figure 2E).

Despite interacting with MEA6, loss of TRAPPC12 did not significantly affect the distribution of Mea6 in CG4 cells (Figure S2A), but it resulted in a significantly dispersed distribution of SEC31A and SEC13 (Figure S2A). Meanwhile, the expression of Mea6, but not other

COPII-related proteins including TANGO1, SEC31A, and SEC13, was significantly downregulated in *Trappc12* KO cells (Figure S2B). Taken together, these results demonstrate that TRAPPC12 interacts with COPII components and controls their distribution. It can speculate that TRAPPC12 downregulation caused by *Mea6* deletion might be associated with impaired oligodendrocyte differentiation and corpus callosum development.

Mea6 is required for CG4 differentiation and maturation

Because Mea6 interacts with TRAPPC12 and they are likely to regulate each other's expression, we employed CRISPR-Cas9 technique to eliminate *Mea6* in CG4 cells to explore Mea6's function in the development of oligodendrocytes. Compared to control cells, KO cells exhibited much less complex branching and lower survival rates during differentiation (Figure 3A). Western blot analysis revealed the complete absence of MBP and a decreased expression of CNP in *Mea6* KO cells following 7 days' differentiation (Figures 3B and 3C).

Mea6 is involved in the organization of COPII lattices and the subsequent formation of trafficking vesicle.[9,22–24] Knockout of *Mea6* in various tissues or cell lines affects the expression of COPII components and cargo transportation.[18,19,22,23,25] We performed electron microscopy analysis and detected the dilation of ER in *Mea6*-KO CG4 cells (Figures S3A and S3B). Meanwhile, we observed a downregulation of SEC31A expression during their proliferation stage (Figure 3D). Immunostaining of SEC31A also showed a significantly reduced fluorescence signal and puncta numbers in KO cells (Figures 3E and 3F). Our previous proteomic results implicated that TRAPPC12 might be downregulated in *Mea6* cKO neurons.[19] We confirmed by Western blot that TRAPCC12 expression was significantly downregulated in *Mea6* KO CG4 cells (Figure 3D). However, SEC13 and another component of the TRAPPIII complex, TRAPPC2,[26] were not significantly downregulated (Figure 3D), indicating the selective downregulation of transporting proteins.

Conditional *Mea6* deletion in OLs causes hypomyelination in mice

To elucidate the physiologic functions of Mea6 in oligodendrocyte development. We ablated *Mea6* in oligodendrocytes by crossbreeding *Mea6*$^{fl/+}$*; Olig2-Cre* mice with *Mea6*$^{fl/fl}$ mice to generate *Mea6* conditional knockout (cKO) mice.[20] Despite no discernible abnormalities in brain morphology, the 4 and 5-month-old cKO mice displayed significantly lower brain weights (Figure 4A). *Mea6* cKO mice also exhibited reduced body weights at 2 to 3 months old (Figure 4B).

Deletion of *Mea6* in OLs causes thinner corpus callosum in mice,[20] implicating the abnormality of myelination. To confirm this, brain slices from adult (Postnatal day 160, P160) mice were stained with Black Gold II dye. *Mea6* cKO mice showed significant hypomyelination in multiple brain regions, including the cortex, corpus callosum (Figure 4C), and hippocampus (Figures S4A and S4B), compared with controls. Consistent with these findings, the expression levels of myelin sheath markers, MBP and CNP, were significantly reduced in the corpus callosum of cKO mice (Figure 4D). Furthermore, the immunostaining intensity of MBP in the cortex and corpus callosum was noticeably lower (Figures S4C and S4D). These results indicate that Mea6 may be essential for oligodendrocyte development and/or the myelination process.

Myelin ultrastructure in corpus callosum was visualized by transmission electron microscopy (TEM) analysis of P160 mice (Figure 4E). The percentage of axons sheathed by myelin was significantly reduced in *Mea6*-cKO mice (62.73% in mutants vs. 28.77% in controls) (Figure 4F). The g-ratio (the ratio of the inner to the outer diameter of the myelin sheath) in the midline of the corpus callosum was significantly increased in cKO mice (0.653 ± 0.089 in WT vs. 0.734 ± 0.096 in cKO), especially for the smaller-diameter axons (Figure 4G). Meanwhile, much more smaller-diameter axons were observed in the cKO group in support of the notion that oligodendrocytes and/or myelination regulate axonal growth (Figure 4E). As predicted, this change was notably rescued by transgenic expression of human *MEA6* (Figures 4E–4G), including elevated expression of MBP and CNP (Figures S4E and S4F).

Increased g-ratio might result from oligodendrocyte immaturity or low complexity. Indeed, the morphological complexity and area of *Mea6*-cKO OPCs cultured for 6 days under differentiating conditions were significantly smaller than controls (Figure 4H). Thus, these findings demonstrate that Mea6 is important for myelination.

Astrocyte activation was observed frequently in various neurodegenerative diseases.[27,28] Through immunostaining, we detected significantly larger cell bodies and more robust branches of astrocytes in the corpus callosum of cKO mice (Figure S5A). Consistent with this observation, the expression levels of GFAP were significantly elevated in the corpus callosum of cKO mice (Figure S5B).

We then examined the expression of COPII and TRAPP complex-related proteins in the corpus callosum (Figures S6A and S6B). We observed similar but a slight difference between CG4 and P160 tissues. Consistent with the observation in CG4 cells, protein levels of TRAPPC12, but not TRAPPC2, were significantly reduced (Figure S6B). SEC13 showed a more significantly decreased expression than SEC31A in *Mea6*-cKO mice (Figure S6A). Both SAR1-GTP, the activated form of SAR1, and total SAR1 displayed significantly elevated levels in *cKO* corpus callosum (Figures S6A and S6B). Taken together, these findings indicate that Mea6 may influence differentiation, maturation, and myelination by affecting the assembly of COPII and/or TRAPP complexes in oligodendrocytes.

Abnormal behaviors and synaptic function in cKO mice

Patients with myelin deficiency frequently show defects in social interaction, movement, learning, and memory. To characterize the physiological function of MEA6 in oligodendrocytes, we inspected various behaviors in 5-month-old cKO mice and their wild-type littermates. Significantly elevated levels of nonsocial anxiety-like behaviors, avoiding the center during the open field test in cKO mice (Figures 5A and 5B). Intriguingly, cKO mice displayed significantly higher social behavior levels in the ultrasonic vocalization (USV) test (Figures 5C and 5D). Specifically, female conspecifics evoked stronger responses, including frequency and duration of communication, in 5-month-old cKO male mice

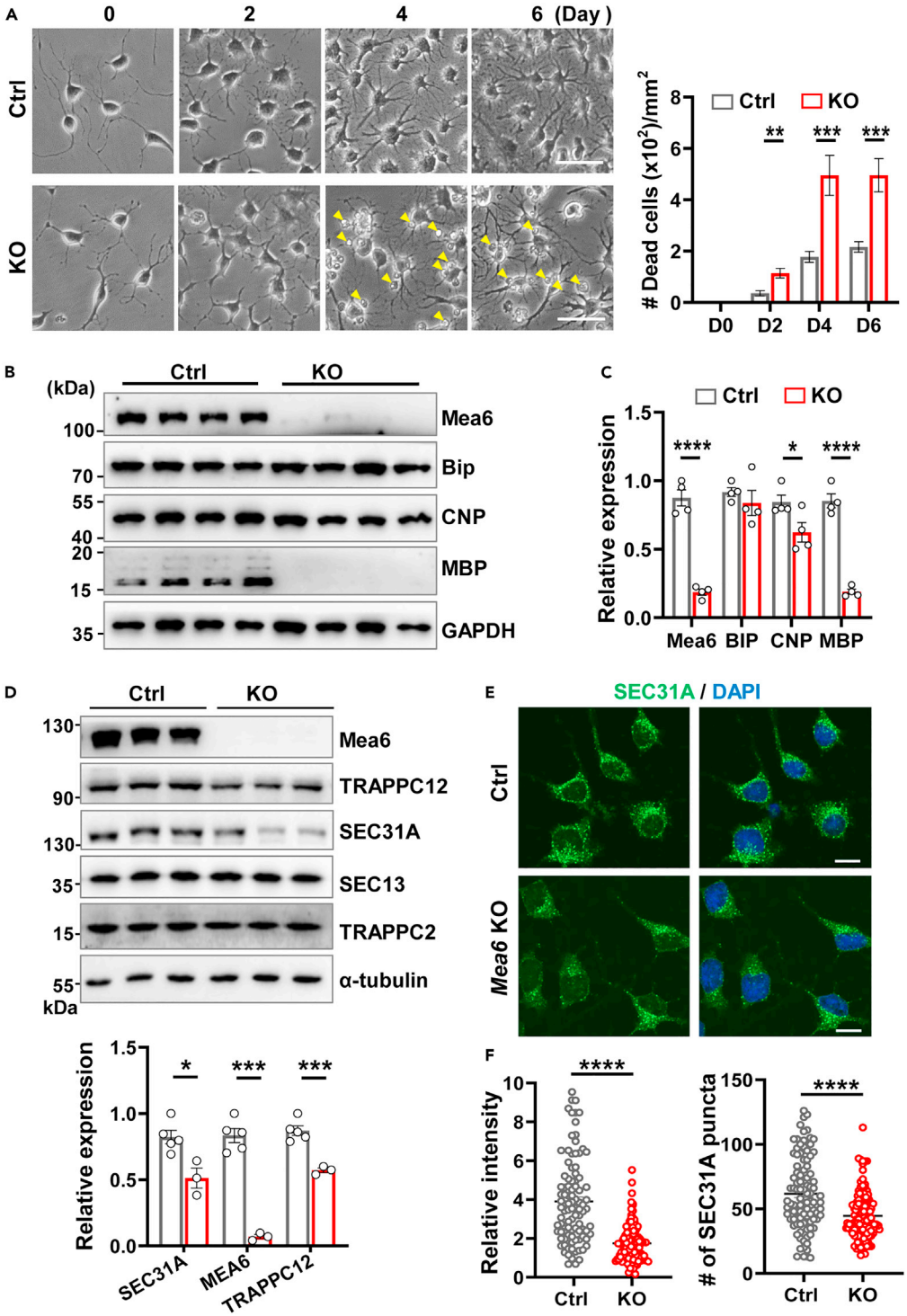

Figure 3. Mea6 regulates OL differentiation *in vitro*

(A) Representative images of CG4 cell morphology and dead cells during differentiation. Arrowheads indicate dead cells. Scale bars: 100 μm.

(B and C) Immunoblotting (B) and quantification (C) of the indicated protein levels in cultured CG4 cells 6 days after differentiation. Five KO samples originated from distinct single clones.

(D) Immunoblotting and quantification of indicated proteins in different WT and *Mea6* KO CG4 clones.

(E) Immunostaining for SEC31A in WT and *Mea6* KO CG4 cells. Scale bar: 10 μm.

(F) Reduced signal and puncta number of SEC31A in *Mea6-KO* cells. Data represent the mean ± SEM. *p < 0.05, **p < 0.01, ***p < 0.001, ****p < 0.0001, Two-tailed unpaired Student's *t* test.

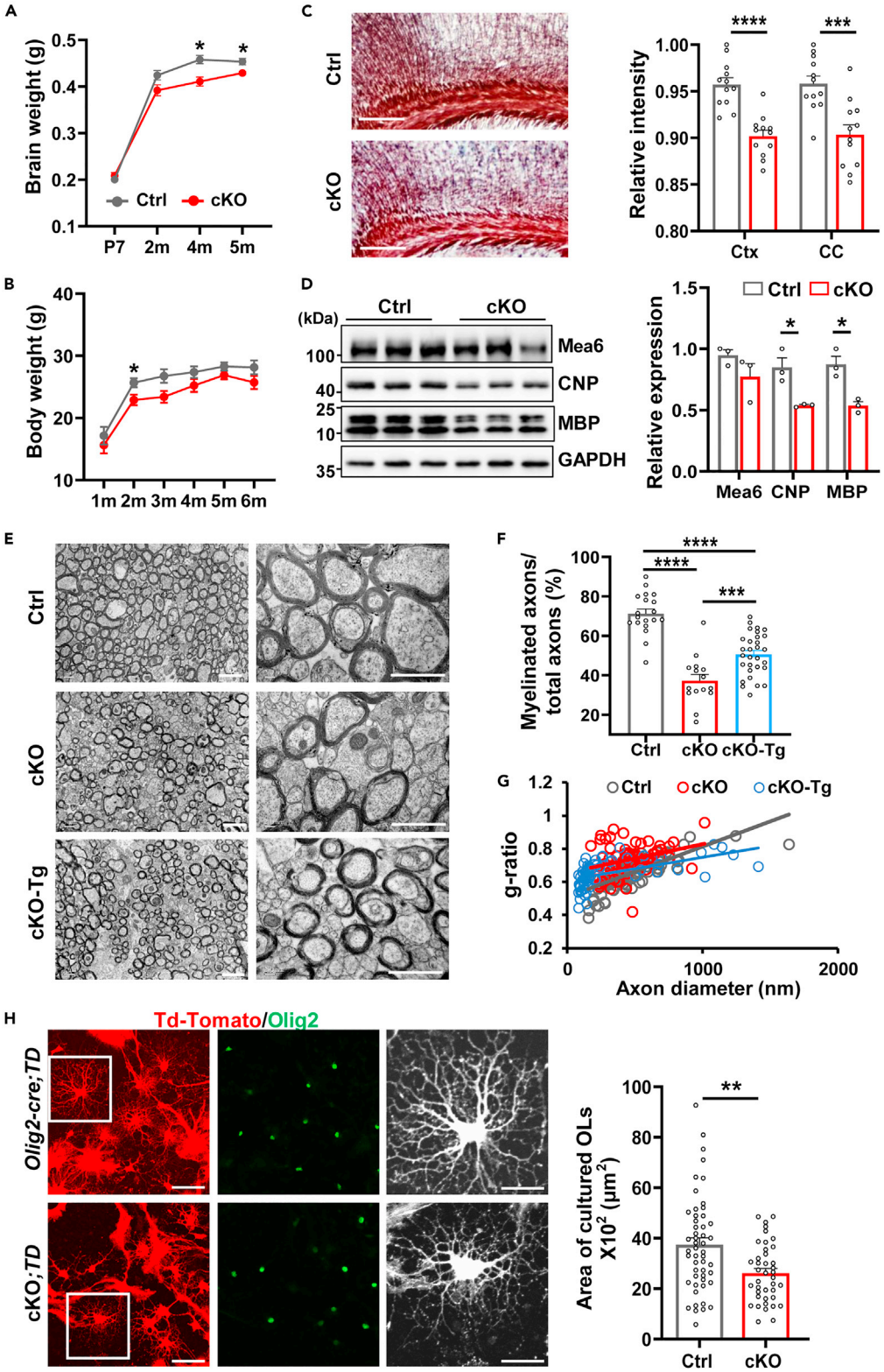

Figure 4. *Mea6*-cKO results in hypomyelination in the brain

(A and B) Reduced brain (A) and body (B) weight in *Mea6*-cKO mice (A: n = 7–12; B = 12–23 animals for each group).

(C) Black gold II staining and quantification of signal intensity in the corpus callosum of P160 mice. ctx: cortex; cc: corpus callosum. Scale bars: 100 μm.

Figure 4. *Continued*

(D) Immunoblotting and quantification of Mea6, CNP and MBP levels in the corpus callosum.

(E) Electron micrographic images of the corpus callosum in control, *Mea6*-cKO, and cKO-Tg mice at P160. Tg indicates the expression of human MEA6. Scale bars: 2 μm and 1000 nm.

(F) The ratio of myelinated axons to total axon count in (E).

(G) Myelin g-ratio in (E). (C-G, n = 3 animals per group).

(H) Immunostaining and quantification of $Olig2^+$ cell morphology and area in cultured primary mouse OPCs following 6 days of differentiation in Ctrl and cKO groups. Td-tomato is expressed in the presence of Cre. Inset figures represent magnified images. (n = 3 independent experiments). Scale bars: 100 μm, insets: 50 μm. Data represent the mean ± SEM. *p < 0.05, **p < 0.01, ***p < 0.001, ****p < 0.0001, two-way ANOVA Sidak multiple comparisons test for (A) and (B); One-way ANOVA with Bonferroni correction test for (F); Two-tailed unpaired Student's *t* test for (C), (D) and (H).

than controls (Figures 5C and 5D). However, there is no significant difference between the two groups in social interaction during the 3-chamber test (Figures S7A and S7B).

We evaluated the mice's movement capacity through open field exploration, rotarod, and beam walking tests. No discernible defect was observed in *Mea6-cKO* mice (Figures 5A, 5B, S7C, and S7D). In addition, no significant defects in short-term and long-term learning/memory were detected during Y maze and water maze tests (Figures S7E–S7H).

Since severe hypomyelination within the hippocampus was detected in cKO mice (Figure S4A), we went on evaluate the synaptic function of the CA1 region (Figure 5E). Recordings from hippocampal slices of *Mea6*-cKO (P160) mice revealed significantly reduced fEPSPs in the stratum radiatum at all stimulation intensities tested than controls (Figures 5F and 5G). Additionally, we inspected the presynaptic release probability (PPF), a form of presynaptic Ca^{2+}-dependent short-term plasticity reflecting the probability of neurotransmitter vesicle release, and found that *Mea6* deletion had significant effects on PPF at varying inter-pulse intervals, including 20, 50, 100, 200, and 400 ms (Figures 5H and 5I). To evaluate if the synaptic function was also influenced at earlier stages, we recorded the consistent indicators of the ventral CA1 region (Figure S8A) in 2-month-old mice. Similar defects in fEPSPs and PPF were detected in cKO mice (Figures S8B–S8E). Taken together, our findings indicate that long-term myelination deficit caused by *Mea6* deficiency affects the synaptic vesicle release process and behaviors.

OL proliferation and differentiation are impaired in *Mea6-cKO* mice

Insufficient myelination could result from a decrease in the number of OLs, insufficient differentiation or maturation, and degeneration of neurons. Therefore, we injected BrdU intraperitoneally to inspect the proliferation of OPC at P6-P7 and detected a lower ratio of $BrdU^+Olig2^+$ cells to $Olig2^+$ cells in the corpus callosum of *Mea6*-cKO than in controls (Figures 6A and 6B). Consistent with this, the density of $Olig2^+$ cells in the corpus callosum was significantly reduced in cKO group (Figure 6C).

Maturation of OLs has obvious regional-specific diversity. We focused on the corpus callosum around P10, a period of rapid oligodendrocyte maturation and onset of myelination.[29,30] To determine if hypomyelination was due to impairment of OL differentiation, we quantified MBP^+ cells in the middle of corpus callosum at P7. The density and complexity of MBP^+ cells were significantly decreased in cKO group (Figures 6D and 6E). We also examined the number of premyelinating and myelinating OLs marked by adenomatous polyposis coli APC (CC1). The ratio of $CC1^+/Olig2^+$ cells and the intensity of $CC1^+$ cells were significantly lower in cKO mice (Figures 6F, 6G, and S9A). We also analyzed myelin ultrastructure at P14 (Figure 6H) and detected the significantly reduced number (Figure 6I) and increased g-ratios (Figure 6J) of myelinated axons in the corpus callosum in cKO mice (0.745 ± 0.052 in WT vs. 0.826 ± 0.063 in cKO). However, no significant change in CNP and MBP was observed in cKO mice at P14 (Figure S9B), probably because myelin formation just gets started around P14. Together, these findings demonstrate that Mea6 is required for the development of OL, including proliferation, differentiation, and maturation in the brain.

Knockout of *Mea6* results in blocked secretion of PTN

A recent study revealed the necessity of SEC13 for oligodendrocyte development, with Sec13 participating in the secretion of pleiotropic protein PTN and influencing oligodendrocyte differentiation.[31] We hypothesized that *Mea6* KO might disturb the differentiation of oligodendrocytes by affecting the secretion of PTN. We examined and found that the expression of PTN in the corpus callosum peaked around P7 (Figure S10A), corresponding to the onset of myelination. As expected, we observed very significant intracellular accumulation of PTN in cultured *Mea6*-cKO immature oligodendrocytes (Figures 7A and 7B). The retention was confirmed by western blot analysis (Figure S10 B). We went on to inspect PTN in the corpus callosum. Low levels of PTN were present in WT mice, but dramatically higher levels were detected in cKOs. Importantly, PTN levels returned to even lower levels in cKO-Tg mice (Figure 7C). These results demonstrate that MEA6 is essential for the secretion of PTN.

To determine whether the defect in PTN secretion is responsible for the disturbed differentiation of *Mea6*-cKO oligodendrocytes, we supplemented PTN to cultured OPCs. PTN significantly enhanced the differentiation of cKO cells (Figures 7D and 7E). Interestingly, we observed many vesicular structures on the branches in both control and cKO cells after treatment with PTN (Figure 7D). Such vesicular structures have been reported in mouse oligodendrocytes overexpressing CNP.[12] Taken together, our findings indicate that PTN retention contributes to disturbed oligodendrocyte differentiation in *Mea6-cKO* mice.

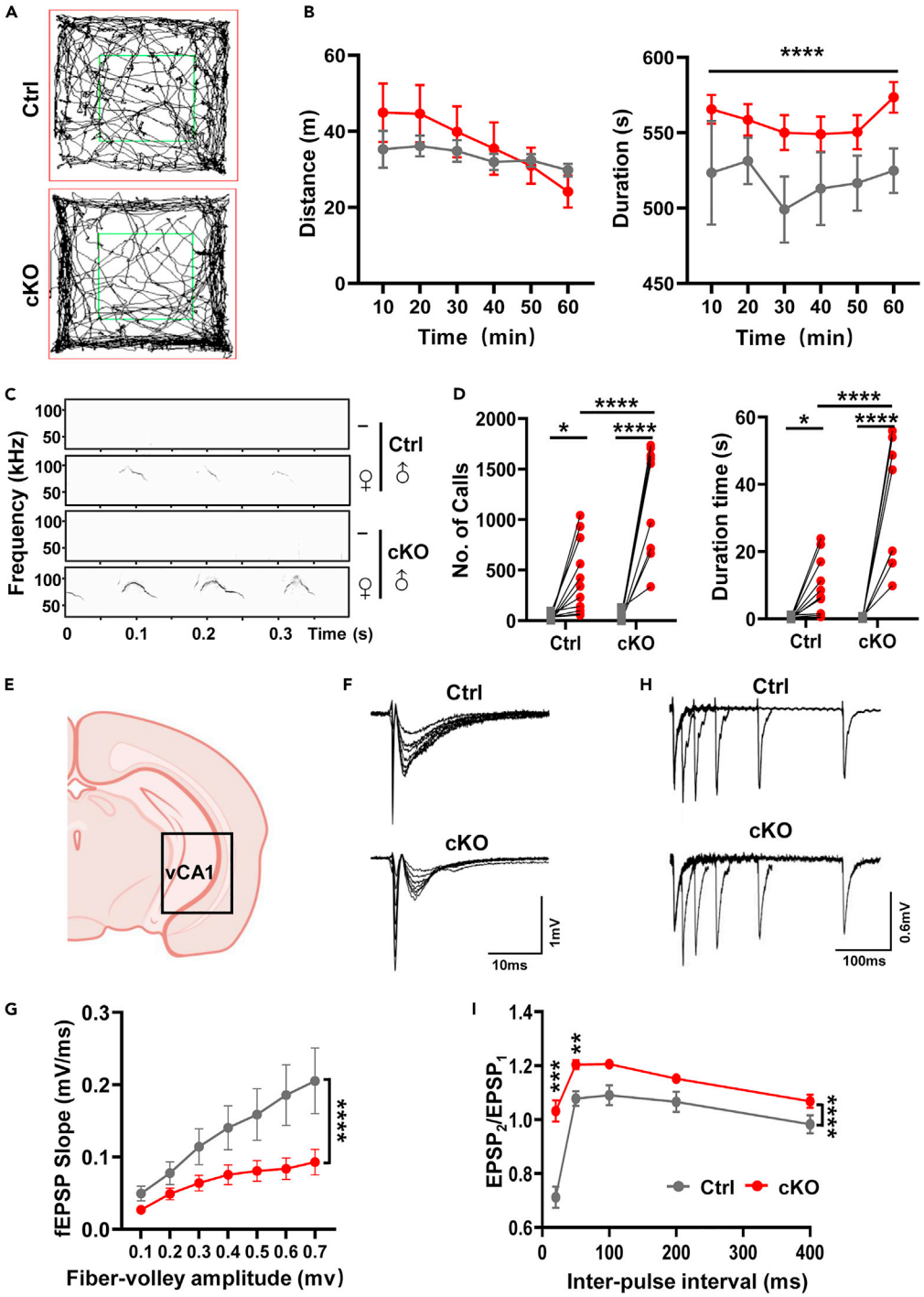

Figure 5. Behavioral and neuronal electrophysiology deficits in *Mea6*-cKO mice at P160

(A) Representative traces in the open field.

(B) cKO mice exhibit normal total exploration distance but increased anxiety-like behaviors. n = 9 control, n = 10 cKO.

(C and D) *Mea6*-cKO mice exhibit hypersocial communication during USV analysis. (C) Representative spectrographs of ultrasonic calls for *Mea6*-cKO mice and controls. (D) Quantitative analysis of number of calls and duration. n = 11 control, n = 9 cKO.

(E–I) *Mea6* OL-cKO affects synaptic function at P160. (E) Schematic illustration of anatomical locations. The black box is vCA1 of the hippocampus and is the approximate location of the data recording. (F) Representative evoked fEPSPs was recorded in acute brain slices. (G) Input-output curves demonstrated a significantly decreased fEPSP slope in *Mea6-cKO*s relative to controls. (n = 7 slices from 2 mice in each group). (H) Representative traces of paired-pulse EPSPs at 20-400 ms interpulse intervals. (I) The pair pulse ratio at all interpulse intervals significantly increased in *Mea6-cKO*s (n = 9 slices from 2 mice in each group). Data represent the mean ± SEM. *p < 0.05, **p < 0.01, ***p < 0.001, ****p < 0.0001, two-way ANOVA Sidak multiple comparisons test.

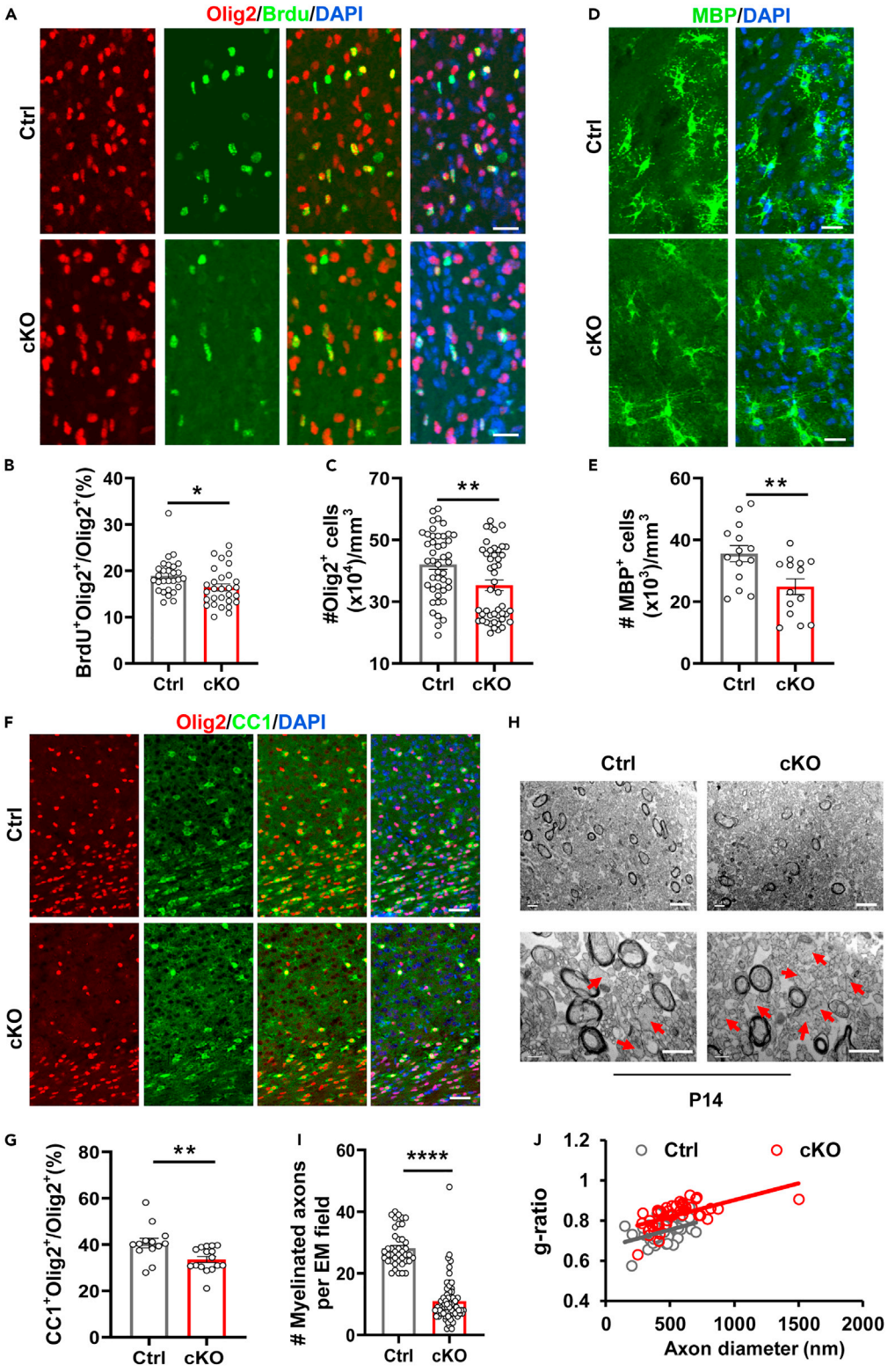

Figure 6. Mea6 controls proliferation and differentiation of the oligodendrocyte lineage

(A) Representative immunostaining of proliferating OLs in the corpus callosum of P7 mice. Scale bar: 20 μm.

(B) Quantification of proliferating OLs ($BrdU^+Olig2^+$) relative to the total number of OLs ($Olig2^+$) 24 h after BrdU labeling.

(C) density of $Olig2^+$ cells. (n = 4 animals per group).

Figure 6. *Continued*

(D and E) Immunostaining for MBP^+ cell (D) and quantification of cell density (E) in the mid-region of the corpus callosum at P7. (n = 3 animals per group). Scale bar: 20 μm.

(F and G) Representative immunostaining of differentiated OLs ($CC1^+$) and total OLs ($Olig2^+$) (F) and quantification of $CC1^+Olig2^+$ cells over the total number of OLs ($Olig2^+$) (G) in the middle part of corpus callosum from P14 mice. (n = 3 animals per group). Scale bar: 40 μm.

(H–J) Hypomyelination in P14 cKOs. Representative EM images of corpus callosum (H). Red arrows indicate large-diameter axons lacking myelination. Scale bars: 2 μm and 1 μm. (I) Quantification of total myelinated axons per EM field (n = 3 animals per group). (J) Linear correlation of g-ratio versus axon diameter (n = 3 animals per group). Data represent the mean ± SEM. *p < 0.05, **p < 0.01, ****p < 0.0001, Two-tailed unpaired Student's *t* test.

DISCUSSION

Upon commencing myelination, oligodendrocytes swiftly synthesize large quantities of proteins and lipids, and transport them to the expanding surface. Dysplasia of white matter was found in patients with *TRAPPC12* mutations.[16,17] The abnormal differentiation and maturation of oligodendrocytes with *Trappc12* deficiency shown in this study provide more evidence that *TRAPPC12* mutations are directly associated with white matter lesions in patients. Importantly, *Mea6* cKO within oligodendrocytes lineage results in white matter dysplasia, as well as reduced expression of Trappc12 in the corpus callosum. *Mea6* removal impedes the proliferation and differentiation of OPCs, and maturation of oligodendrocytes, culminating in hypomyelination and aberrant behaviors. Some of these behaviors, such as hyper-sociability and increased non-social anxiety levels, are reminiscent of Williams syndrome patients who have likewise been documented to exhibit white matter dysplasia.[8,32] Mechanically, elimination of *Mea6* in oligodendrocytes is likely to disrupt the early secretory pathway, including components of the COPII and potentially TRAPP complex, thereby inhibiting PTN secretion and differentiation of OPCs (Figure 8).

Importantly, we found that TRAPPC12 interacts with MEA6 and knockout of *Trappc12* leads to reduced expression of Mea6 in CG4 cells. As a constituent of the TRAPPIII complex, TRAPPC12 has been shown to interact with the COPII outer layer.[21] We verified that TRAPPC12 can interact with SEC31 and SEC13, and regulate the cellular distribution of both SEC13 and SEC31 in CG4 cells. Interestingly, *Trappc12* deficiency exerts a more pronounced impact on the distribution of SEC13/31 than *Mea6* deficiency. It may be because TRAPPC12 is still present on the vesicles of COPII and stabilize the coats after budding from ERES. Deletion of *Trappc12* reduces the complexity of differentiated CG4 cells. This supports the notion that the decreased Trappc12 expression caused by *Mea6* deletion may contribute to blocked oligodendrocyte differentiation. Beyond Trappc12, the expression of COPII components was dysregulated in the *Mea6* cKO corpus callosum, typified by downregulated levels of SEC13 and SEC31A, and upregulated levels of SAR1-GTP and total SAR1. These alterations parallel those observed in the *Nestin-cre Mea6* cKO cortex,[19] indicating the analogous function of MEA6 in neurons and oligodendrocytes.

Mea6 interacting protein, TANGO1, has been shown to interact with TRAPPC2/Sedlin, and TRAPPC2 knockdown also affects the distribution of various COPII members, efficient cycling of Sar1 and vesical trafficking.[26] We, therefore, propose that Mea6 and TANGO1 interact with each other and different components of the TRAPP complex at the ER exit site, in addition to COPII components, to control the ER-Golgi trafficking (Figure 8).

Although the secretion of PTN is severely blocked in *Mea6*-deficient oligodendrocytes similar to *Sec13*-KO OLs, PTN can only partially ameliorate the abnormal differentiation engendered by *Mea6* deletion. This phenomenon can be attributed to the fact that PTN is predominantly expressed in the pre-mature stage of OLs,[31] while Mea6 is expressed throughout the OL lineage. Thus, PTN could partially rescue differentiation but not oligodendrocyte maturation after *Mea6* ablation. In addition to PTN, the trafficking of other cargoes regulated by MEA6 may also play a role in oligodendrocyte differentiation and maturation.

In summary, we show that TRAPPC12 and Mea6 interact with each other to govern oligodendrocyte development by influencing the ER-to-Golgi vesicle trafficking, and elucidated the potential underlying mechanism. These insights will enhance our understanding of white matter and neuronal disorders.

STAR★METHODS

Detailed methods are provided in the online version of this paper and include the following:

- KEY RESOURCES TABLE
- RESOURCE AVAILABILITY
  - Lead contact
  - Materials availability
  - Data and code availability
- EXPERIMENTAL MODEL AND STUDY PARTICIPANT DETAILS
  - Animals
- METHOD DETAILS
  - OPC isolation, cell cultures & CRISPR technology
  - CG4 cell area statistic
  - Recombinant virus production
  - Co-IP, western blotting and gray statistics
  - Perfusion and immunostaining analysis
  - Black gold II staining

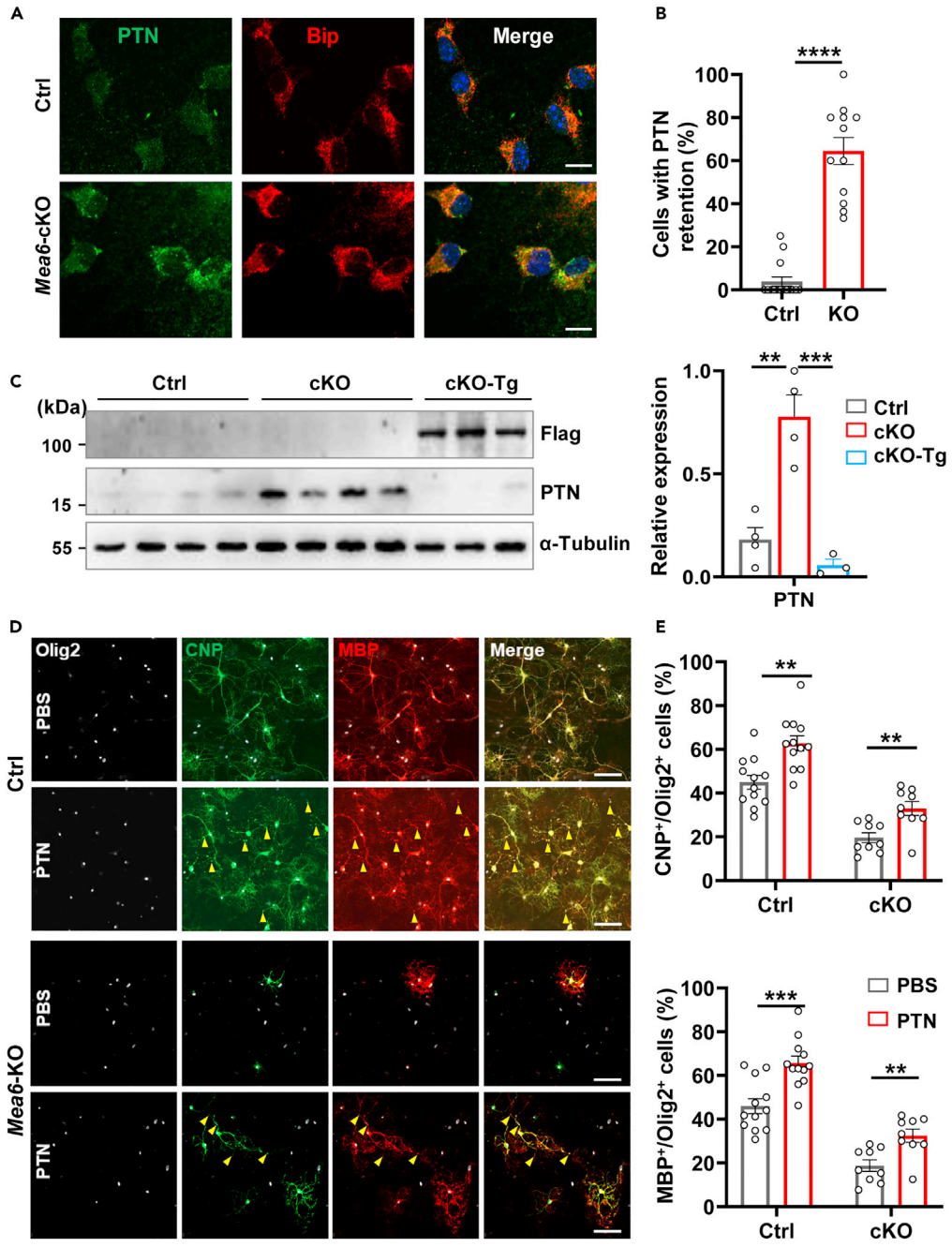

Figure 7. PTN can enhance the differentiation of *Mea6*-cKO OPCs

(A and B) Immunostaining and intensity quantification of PTN in primary cultured OPCs. Each sample is from different mice. Scale bar: 10 μm.

(C) Immunoblot and quantification show increased PTN levels in *Mea6*-cKO corpus callosum at P160. α-Tubulin serves as loading control.

(D) Immunostaining of Olig2, CNP, and MBP in cultured primary OLs after 6 days of differentiation and treated with PBS or 100 μM PTN. The yellow triangle indicates protein aggregates. Scale bar: 100 μm.

(E) Quantification of the percentage of CNP^+ or MBP^+ cells over $Olig2^+$ (n = 4 animals in each group). Data represent the mean ± SEM. **p < 0.01, ***p < 0.001, ****p < 0.0001, One-way ANOVA with Bonferroni correction test for (C); Two-tailed unpaired Student's *t* test for both (B) and (E).

- ○ Transmission electron microscopy (TEM) and statistical analysis
- ○ BrdU incorporation assay
- ○ Electrophysiology and statistical analysis
- ○ Behavioral assessment and statistical analysis

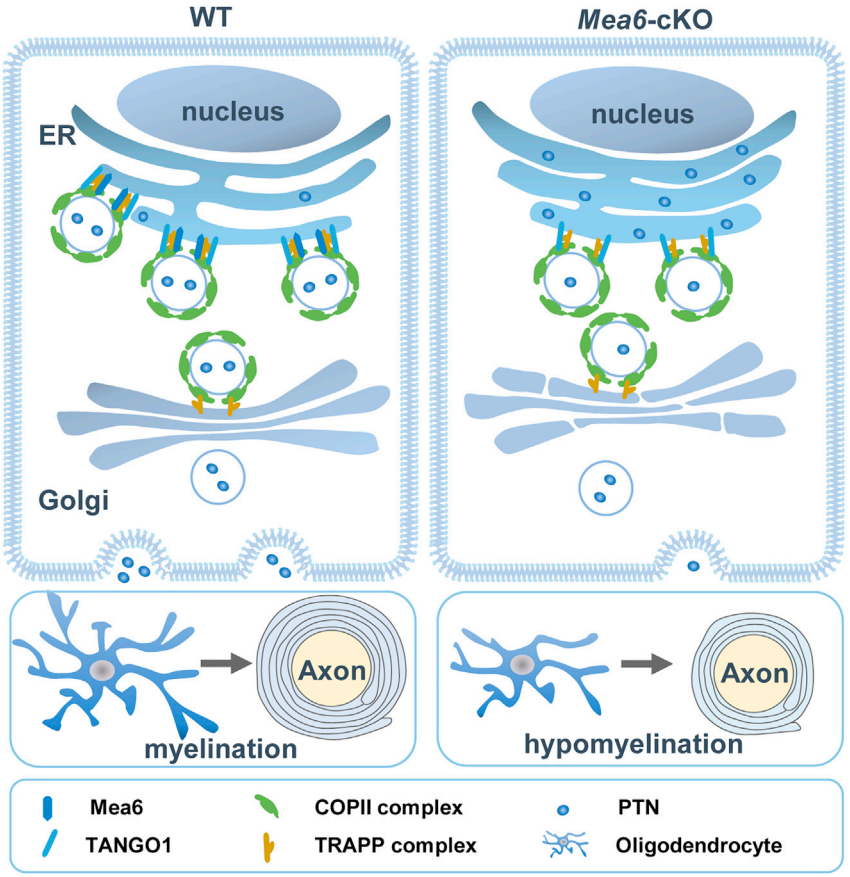

Figure 8. Schematic illustration of the mechanism by which Mea6 and TRAPP complex regulate myelination in the brain

Mea6 interacts with TRAPP components to regulate cargo transport pathway in the oligodendrocyte lineage. Loss of *Mea6* results in reduced levels of certain COPII and TRAPP components, leading to cargo retention in the ER, including PTN, and enlargement of the ER lumen. Reduced PTN secretion leads to defects OPC proliferation, oligodendrocyte differentiation, and maturation, resulting in hypomyelination.

SUPPLEMENTAL INFORMATION

Supplemental information can be found online at https://doi.org/10.1016/j.isci.2024.109180.

ACKNOWLEDGMENTS

We thank Dr. Mengsheng Qiu for providing CG4 cells and Dr. Weixiang Guo for CAG-Pr-loxP-Stop-loxP-TD-tomato transgenic mice. We also thank Ting Li for flow cytometry support and Lin Yang for discussion of TEM details. This study was supported by the National Key R & D Program of China (MOST, 2022YFC3600200, 2021ZD0202300) and the National Science Foundation of China (91854118, 32330038, 31921002, 32394030, and 32061143026), and Chinese Academy of Sciences (YJKYYQ20200052).

AUTHOR CONTRIBUTIONS

Z.X., Y. W. and T.M. conceived and supervised the project. T.M. conducted most of the experiments and analyzed the results. L.Y. and Z.L. designed and performed electrophysiology experiments. T.M., Y.W. and T.W. did TEM analysis. T.M., P.S., and K.H. designed and performed the CRISPR experiment. T.M. and X.Z. wrote the manuscript. All of the authors discussed the results and commented on the manuscript.

DECLARATION OF INTERESTS

The authors declare no competing interests.

Received: July 31, 2023
Revised: November 11, 2023
Accepted: February 6, 2024
Published: February 8, 2024

REFERENCES

1. Salzer, J.L., and Zalc, B. (2016). Myelination. Curr. Biol. *26*, R971–R975. https://doi.org/10.1016/j.cub.2016.07.074.
2. Simons, M., and Nave, K.A. (2015). Oligodendrocytes: Myelination and Axonal Support. Cold Spring Harb. Perspect. Biol. *8*, a020479. https://doi.org/10.1101/cshperspect.a020479.
3. Nave, K.A. (2010). Myelination and support of axonal integrity by glia. Nature *468*, 244–252. https://doi.org/10.1038/nature09614.
4. Nave, K.A., and Werner, H.B. (2014). Myelination of the nervous system: mechanisms and functions. Annu. Rev. Cell Dev. Biol. *30*, 503–533. https://doi.org/10.1146/annurev-cellbio-100913-013101.
5. Wang, F., Ren, S.Y., Chen, J.F., Liu, K., Li, R.X., Li, Z.F., Hu, B., Niu, J.Q., Xiao, L., Chan, J.R., and Mei, F. (2020). Myelin degeneration and diminished myelin renewal contribute to age-related deficits in memory. Nat. Neurosci. *23*, 481–486. https://doi.org/10.1038/s41593-020-0588-8.
6. Wang, F., Yang, Y.J., Yang, N., Chen, X.J., Huang, N.X., Zhang, J., Wu, Y., Liu, Z., Gao, X., Li, T., et al. (2018). Enhancing Oligodendrocyte Myelination Rescues Synaptic Loss and Improves Functional Recovery after Chronic Hypoxia. Neuron *99*, 689–701.e5. https://doi.org/10.1016/j.neuron.2018.07.017.
7. Nasrabady, S.E., Rizvi, B., Goldman, J.E., and Brickman, A.M. (2018). White matter changes in Alzheimer's disease: a focus on myelin and oligodendrocytes. Acta Neuropathol. Commun. *6*, 22. https://doi.org/10.1186/s40478-018-0515-3.
8. Barak, B., Zhang, Z., Liu, Y., Nir, A., Trangle, S.S., Ennis, M., Levandowski, K.M., Wang, D., Quast, K., Boulting, G.L., et al. (2019). Neuronal deletion of Gtf2i, associated with Williams syndrome, causes behavioral and myelin alterations rescuable by a remyelinating drug. Nat. Neurosci. *22*, 700–708. https://doi.org/10.1038/s41593-019-0380-9.
9. Ma, T., Zhang, F., Wang, Y., and Xu, Z. (2022). Molecular mechanisms underlying cTAGE5/MEA6-mediated cargo transport and biological functions. J Genet Genomics *49*, 519–522. https://doi.org/10.1016/j.jgg.2022.04.001.
10. Raote, I., Saxena, S., Campelo, F., and Malhotra, V. (2021). TANGO1 marshals the early secretory pathway for cargo export. Biochim. Biophys. Acta. Biomembr. *1863*, 183700. https://doi.org/10.1016/j.bbamem.2021.183700.
11. Peotter, J., Kasberg, W., Pustova, I., and Audhya, A. (2019). COPII-mediated trafficking at the ER/ERGIC interface. Traffic *20*, 491–503. https://doi.org/10.1111/tra.12654.
12. Yin, X., Peterson, J., Gravel, M., Braun, P.E., and Trapp, B.D. (1997). CNP overexpression induces aberrant oligodendrocyte membranes and inhibits MBP accumulation and myelin compaction. J. Neurosci. Res. *50*, 238–247. https://doi.org/10.1002/(SICI)1097-4547(19971015)50:2<238::AID-JNR12>3.0.CO;2-4.
13. Lord, C., Bhandari, D., Menon, S., Ghassemian, M., Nycz, D., Hay, J., Ghosh, P., and Ferro-Novick, S. (2011). Sequential interactions with Sec23 control the direction of vesicle traffic. Nature *473*, 181–186. https://doi.org/10.1038/nature09969.
14. Yu, S., Satoh, A., Pypaert, M., Mullen, K., Hay, J.C., and Ferro-Novick, S. (2006). mBet3p is required for homotypic COPII vesicle tethering in mammalian cells. J. Cell Biol. *174*, 359–368. https://doi.org/10.1083/jcb.200603044.
15. Abbasi, A.A., Blaesius, K., Hu, H., Latif, Z., Picker-Minh, S., Khan, M.N., Farooq, S., Khan, M.A., and Kaindl, A.M. (2017). Identification of a novel homozygous TRAPPC9 gene mutation causing non-syndromic intellectual disability, speech disorder, and secondary microcephaly. Am. J. Med. Genet. B Neuropsychiatr. Genet. *174*, 839–845. https://doi.org/10.1002/ajmg.b.32602.
16. Milev, M.P., Grout, M.E., Saint-Dic, D., Cheng, Y.H.H., Glass, I.A., Hale, C.J., Hanna, D.S., Dorschner, M.O., Prematilake, K., Shaag, A., et al. (2017). Mutations in TRAPPC12 Manifest in Progressive Childhood Encephalopathy and Golgi Dysfunction. Am. J. Hum. Genet. *101*, 291–299. https://doi.org/10.1016/j.ajhg.2017.07.006.
17. Aslanger, A.D., Demiral, E., Sonmez-Sahin, S., Guler, S., Goncu, B., Yucesan, E., Iscan, A., Saltik, S., and Yesil, G. (2020). Expanding Clinical Phenotype of TRAPPC12-Related Childhood Encephalopathy: Two Cases and Review of Literature. Neuropediatrics *51*, 430–434. https://doi.org/10.1055/s-0040-1710526.
18. Saito, K., Yamashiro, K., Ichikawa, Y., Erlmann, P., Kontani, K., Malhotra, V., and Katada, T. (2011). cTAGE5 mediates collagen secretion through interaction with TANGO1 at endoplasmic reticulum exit sites. Mol. Biol. Cell *22*, 2301–2308. https://doi.org/10.1091/mbc.E11-02-0143.
19. Zhang, F., Wang, Y., Wang, T., Yao, L., Lam, S.M., Huang, X., Fan, J., Wang, Q., Liu, L., Jiang, Y., et al. (2018). cTAGE5/MEA6 plays a critical role in neuronal cellular components trafficking and brain development. Proc. Natl. Acad. Sci. USA *115*, E9449–E9458. https://doi.org/10.1073/pnas.1804083115.
20. Ma, T., Mao, W., Zhang, S., Wang, Y., Wang, T., Liu, J., Shi, L., Yu, X., Xue, R., Shui, G., and Xu, Z. (2023). Ablation of Mea6/cTAGE5 in oligodendrocytes significantly impairs white matter structure and lipid content. Life Metab. *2*. https://doi.org/10.1093/lifemeta/load010.
21. Zhao, S., Li, C.M., Luo, X.M., Siu, G.K.Y., Gan, W.J., Zhang, L., Wu, W.K.K., Chan, H.C., and Yu, S. (2017). Mammalian TRAPPIII Complex positively modulates the recruitment of Sec13/31 onto COPII vesicles. Sci. Rep. *7*, 43207. https://doi.org/10.1038/srep43207.
22. Wang, Y., Liu, L., Zhang, H., Fan, J., Zhang, F., Yu, M., Shi, L., Yang, L., Lam, S.M., Wang, H., et al. (2016). Mea6 controls VLDL transport through the coordinated regulation of COPII assembly. Cell Res. *26*, 787–804. https://doi.org/10.1038/cr.2016.75.
23. Saito, K., Yamashiro, K., Shimazu, N., Tanabe, T., Kontani, K., and Katada, T. (2014). Concentration of Sec12 at ER exit sites via interaction with cTAGE5 is required for collagen export. J. Cell Biol. *206*, 751–762. https://doi.org/10.1083/jcb.201312062.
24. Santos, A.J.M., Nogueira, C., Ortega-Bellido, M., and Malhotra, V. (2016). TANGO1 and Mia2/cTAGE5 (TALI) cooperate to export bulky pre-chylomicrons/VLDLs from the endoplasmic reticulum. J. Cell Biol. *213*, 343–354. https://doi.org/10.1083/jcb.201603072.
25. Fan, J., Wang, Y., Liu, L., Zhang, H., Zhang, F., Shi, L., Yu, M., Gao, F., and Xu, Z. (2017). cTAGE5 deletion in pancreatic beta cells impairs proinsulin trafficking and insulin biogenesis in mice. J. Cell Biol. *216*, 4153–4164. https://doi.org/10.1083/jcb.201705027.
26. Venditti, R., Scanu, T., Santoro, M., Di Tullio, G., Spaar, A., Gaibisso, R., Beznoussenko, G.V., Mironov, A.A., Mironov, A., Jr., Zelante, L., et al. (2012). Sedlin controls the ER export of procollagen by regulating the Sar1 cycle. Science *337*, 1668–1672. https://doi.org/10.1126/science.1224947.
27. Guillamón-Vivancos, T., Gómez-Pinedo, U., and Matías-Guiu, J. (2015). Astrocytes in neurodegenerative diseases (I): function and molecular description. Neurologia *30*, 119–129. https://doi.org/10.1016/j.nrl.2012.12.007.
28. Oksanen, M., Lehtonen, S., Jaronen, M., Goldsteins, G., Hämäläinen, R.H., and Koistinaho, J. (2019). Astrocyte alterations in neurodegenerative pathologies and their modeling in human induced pluripotent stem cell platforms. Cell. Mol. Life Sci. *76*, 2739–2760. https://doi.org/10.1007/s00018-019-03111-7.
29. Dean, J.M., Moravec, M.D., Grafe, M., Abend, N., Ren, J., Gong, X., Volpe, J.J., Jensen, F.E., Hohimer, A.R., and Back, S.A. (2011). Strain-specific differences in perinatal rodent oligodendrocyte lineage progression and its correlation with human. Dev. Neurosci. *33*, 251–260. https://doi.org/10.1159/000327242.
30. Barateiro, A., and Fernandes, A. (2014). Temporal oligodendrocyte lineage progression: in vitro models of proliferation, differentiation and myelination. Biochim. Biophys. Acta *1843*, 1917–1929. https://doi.org/10.1016/j.bbamcr.2014.04.018.
31. Liu, Z., Yan, M., Lei, W., Jiang, R., Dai, W., Chen, J., Wang, C., Li, L., Wu, M., Nian, X., et al. (2022). Sec13 promotes oligodendrocyte differentiation and myelin repair through autocrine pleiotrophin signaling. J. Clin. Invest. *132*, e155096. https://doi.org/10.1172/JCI155096.
32. Nir, A., and Barak, B. (2021). White matter alterations in Williams syndrome related to behavioral and motor impairments. Glia *69*, 5–19. https://doi.org/10.1002/glia.23868.

33. Yoshida, A., Takashima, K., Shimonaga, T., Kadokura, M., Nagase, S., and Koda, S. (2020). Establishment of a simple one-step method for oligodendrocyte progenitor cell preparation from rodent brains. J. Neurosci. Methods *342*, 108798. https://doi.org/10.1016/j.jneumeth.2020.108798.

34. Dugas, J.C., and Emery, B. (2013). Purification of oligodendrocyte precursor cells from rat cortices by immunopanning. Cold Spring Harb. Protoc. *2013*, 745–758. https://doi.org/10.1101/pdb.prot070862.

35. Guo, W., Zhang, L., Christopher, D.M., Teng, Z.Q., Fausett, S.R., Liu, C., George, O.L., Klingensmith, J., Jin, P., and Zhao, X. (2011). RNA-Binding Protein FXR2 Regulates Adult Hippocampal Neurogenesis by Reducing Noggin Expression. Neuron *70*, 924–938. https://doi.org/10.1016/j.neuron.2011.03.027.

36. Xu, Z., Kukekov, N.V., and Greene, L.A. (2003). POSH acts as a scaffold for a multiprotein complex that mediates JNK activation in apoptosis. EMBO J. *22*, 252–261. https://doi.org/10.1093/emboj/cdg021.

37. Schmued, L., Bowyer, J., Cozart, M., Heard, D., Binienda, Z., and Paule, M. (2008). Introducing Black-Gold II, a highly soluble gold phosphate complex with several unique advantages for the histochemical localization of myelin. Brain Res. *1229*, 210–217. https://doi.org/10.1016/j.brainres.2008.06.129.

38. Zhang, H., Kang, E., Wang, Y., Yang, C., Yu, H., Wang, Q., Chen, Z., Zhang, C., Christian, K.M., Song, H., et al. (2016). Brain-specific Crmp2 deletion leads to neuronal development deficits and behavioural impairments in mice. Nat. Commun. *7*, 11773. https://doi.org/10.1038/ncomms11773.

39. Yao, M., Meng, M., Yang, X., Wang, S., Zhang, H., Zhang, F., Shi, L., Zhang, Y., Zhang, X., and Xu, Z. (2022). POSH regulates assembly of the NMDAR/PSD-95/Shank complex and synaptic function. Cell Rep. *39*, 110642. https://doi.org/10.1016/j.celrep.2022.110642.

STAR★METHODS

KEY RESOURCES TABLE

REAGENT or RESOURCE	SOURCE	IDENTIFIER
Antibodies		
Rabbit-*anti*-MEA6/cTAGE5	Sigma	Cat# HPA000387; RRID: AB_1078582
Mouse-*anti*-O4	Millipore	Cat# MAB345; RRID: AB_11213138
Goat anti-mouse IgG + IgM	Jackson ImmunoResearch	Cat# 115-005-044; RRID: AB_2338451
Rat-*anti*-BrdU	Abcam	Cat# ab6326; RRID: AB_2313786
Mouse-*anti*-CC1	Millipore	Cat# OP80; RRID: AB_2057371
Rabbit -*anti*-GFP	Abcam	Cat# ab290; RRID: AB_2313768
Chicken-*anti*-GFP	Abcam	Cat# ab13970; RRID: AB_300798
Mouse-*anti*-GFP	Santa Cruz	Cat# sc-9996; RRID: AB_627695
Rabbit-*anti*-GFAP	Dako	Cat# Z0334; RRID: AB_10013382
Rat-*anti*-MBP	Abcam	Cat# ab7349; RRID: AB_305869
Mouse-*anti*-CNP	Abcam	Cat# ab6319; RRID: AB_2082593
Mouse-*anti*-Olig2	Millipore	Cat# MABN50; RRID: AB_10807410
Rabbit-*anti*-Olig2	Millipore	Cat# ab9610; RRID: AB_570666
Rabbit-*anti*-Bip	Abcam	Cat# ab21685; RRID: AB_2119834
Mouse-*anti*-TRAPPC12	Abnova	Cat# H0005112-P01
Rabbit-*anti*-TRAPPC2	Proteintech	Cat# 12484; RRID: AB_2208136
Rabbit-*anti*-SEC31A	Cell signaling technology	Cat# 13466; RRID: AB_2798228
Rabbit-*anti*-SEC13	Abcam	Cat# ab168824
Rabbit-*anti*-SEC23A	Cell signaling technology	Cat# 8162; RRID: AB_10859891
Mouse-*anti*-PTN	Santa Cruz	Cat# sc-74443; RRID: AB_1128556
Mouse-*anti*-Flag	MBL	Cat# M185; RRID: AB_11123930
Rabbit-*anti*-Myc	MBL	Cat# M562
Mouse-*anti*-HA	MBL	Cat# M180; RRID: AB_10951811
Mouse-*anti*-a-tubulin	Cell signaling technology	Cat# 3873s; RRID: AB_1904178
Mouse-*anti*-GAPDH	Cell signaling technology	Cat# 97166s; RRID: AB_2756824
Mouse-*anti*-β-actin	Cell signaling technology	Cat# 3700s; RRID: AB_2242334
Recombinant DNA		
pEGFP-SEC31A	This laboratory	N/A
pCMV-myc-SEC13	This laboratory	N/A
pCMV-flag-TRAPPC12	This paper	N/A
pCMV-HA-TRAPPC12	This paper	N/A
pCMV-flag-MEA6	This laboratory	N/A
Experimental models: Cell lines		
Mouse oligodendrocyte progenitor cell	This paper	N/A
HEK293	ATCC	Cat# CRL-11268
CG4	Dr. Mengsheng Qiu (Hangzhou Normal University)	N/A
Chemicals, peptides, and recombinant proteins		
Vigofect	Vigorous Biotechnology	Cat# T001
Lipo2000	Thermo Fisher	Cat# 11668019

(*Continued on next page*)

Continued

REAGENT or RESOURCE	SOURCE	IDENTIFIER
Poly- D -lysine (PDL)	Sigma-Aldrich	Cat# P7280
PTN	SinoBiological	Cat# 51000-MNAB
Insulin	Sigma-Aldrich	Cat# I6634
Dithiothreitol (DTT)	Sigma-Aldrich	Cat# D9760
B-27 Supplement	Gibco	Cat# 17504-044
N-2 Supplement	Gibco	Cat# A1370701
EGF	Peprotech	Cat# AF-100-15-100
PDGFRα	Peprotech	Cat# 100-13A
Holo-transferrin	Sigma-Aldrich	Cat# T1147
CNTF	Peprotech	Cat# AF-450-50
progesterone	Sigma-Aldrich	Cat# P8783
putrescine	Sigma-Aldrich	Cat# P5780
T3	Sigma-Aldrich	Cat# T6397
Bacterial and virus strains		
DH5a	Tiangen	Cat# CB101-02
Lentivirus	This paper	N/A
Microsoft and software		
LSM 700	Carl Zeiss	N/A
ImageJ	NIH	RRID:SCR_003070
SMART Video-tracking	Panlab	RRID:SCR_002852
GraphPad Prism 8.0.2	GraphPad	

RESOURCE AVAILABILITY

Lead contact

Further information and any related requests should be directed to and will be fulfilled by the lead contact, Professor Zhiheng Xu (zhxu@genetics.ac.cn).

Materials availability

This study did not generate new unique reagents.

Data and code availability

The datasets and images generated during this study are available from the lead contact upon request.

This paper does not report original code.

Any additional information required to reanalyse the data reported in this paper is available from the lead contact upon request.

EXPERIMENTAL MODEL AND STUDY PARTICIPANT DETAILS

Animals

Mea6$^{fl/fl}$ mice and *MEA6* transgenic mice were previously generated.[22] Briefly, the flanking of the 11th exon in the Mea6 gene was inserted in two *loxP* sites. For *MEA6* transgenic *mice*, CAG promoter, LoxP-Stop-LoxP element (for conditional expression under the control of Cre), 3 x Flag-tagged human MEA6 containing P521A point mutation. CAG-Pr-loxP-Stop-loxP-*MEA6*-(P521A)-3 x Flag-WPRE-pA fragments were inserted in Rosa26 site through homologous recombination.[19] Mea6 was specifically deleted in oligodendrocytes by crossing *Mea6*$^{fl/fl}$ mice with mice expressing Cre recombinase as a knock-in gene into *Olig2*. We crossed *hMEA6-Tg; Mea6*$^{fl/+}$ mice with *Mea6*$^{fl/+}$*; Olig2-Cre* mice to generate *hMEA6-Tg; Mea6*$^{fl/fl}$*; Olig2-Cre* (cKO-Tg mice). *Mea6-GFP-KI* mice were constructed by our group and company. Briefly, we insert the sequence around the last axon of *Mea6* in the genome that can encode the EGFP protein. We identify our mouse by sequencing, immunostaining, and western blot. TD-tomato mice were a gift from Weixiang Guo in our institute. TD-tomato mice were constructed by inserting CAG-Pr-loxP-Stop-loxP-TD-tomato in Rosa26 site, which means only Cre can induce the expression of this reporter gene. To get two groups of TD-positive OPC, we cross the *Mea6*$^{fl/+}$; TD with *Mea6*$^{fl/+}$; *Olig2-Cre* mice. Paw biopsies were used to extract genomic DNA for genotyping

about one week after birth. All animal experiments were performed based on the protocols which were approved by the Institutional Animal Care and Use Committee at the Institute of Genetics and Developmental Biology, Chinese Academy of Sciences.

METHOD DETAILS

OPC isolation, cell cultures & CRISPR technology

The oligodendrocyte progenitor cells were isolated from P0 to P3-*d*-old wild-type and conditional knockout pups as previously described.[33,34] Briefly, the cortex from P0-P3 mice was dissected and dissociated with accutase for 13 min at 37°C. Blow into single-cell suspension and then seeded onto the poly-D-lysine coated coverslips in proliferation medium (DMEM/F12 supplemented with 2% B-27 supplement, 1% N-2, 10 ng/mL EGF, 10 ng/mL PDGFRα and 1% GlutaMAX). The culture dish must be shaken to suspend the cell debris the next day, and then replaced with fresh culture medium. After that, the medium should be half replaced with a fresh medium every 2 days. When the cells reach the proper density, the medium was changed to the DMEM supplemented with 2% B-27 supplement, 5 μg/mL insulin, 1% GlutaMAX, 10 mg/mL Holo-transferrin, 0.5% FBS, 50 ng/mL CNTF, and 1% 100 × OL-supplement for the differentiation. 100 × OL-supplement: 1.02 g BSA, 0.6 mg progesterone, 161 mg putrescine, 0.05 mg sodium selenite, and 4 mg T3 dissolved into 100 mL DMEM. Oligodendrocytes were identified by immunofluorescence staining for lineage marker Olig2 and the purity reaches more than 90%.

To generate CG4 cell lines in which Mea6 or TRAPPC12 expression was abolished, we choose the CRISPR/Cas9 system. Briefly, we design sgRNAs in the second axon of *Mea6* or *Trappc12* through the CRISPOR-TEFOR (https://tefor.net/portfolio/crispor) and insert them in the PX458 plasmid. After 24 h transfection with Lipo3000, GFP-positive CG4 cells were isolated by FACS, and single cells were seeded onto poly-D-lysine coated 96-well plates. Medium conditions are consistent with those of primary OPC cells. Sequencing and western blot were used to verify knockout efficiency. A total of HEK293 cells were cultured in DMEM supplemented with 10% FBS, and HEK293, HEK293T, cells were transiently transfected with Vigofect. All cells were cultured at 37°C with 5% CO_2.

The sgRNA sequences for knockout Trappc12 are as follows:

sgRNA1: GACTCTCCGAACAACAGCGA
sgRNA2: CCACAGACTGCCCGATAGCA

CG4 cell area statistic

CG4 cells cultured on a 24-well plate were imaged using a bright field microscope at different times of differentiation, including D0, D2, D4, and D6. Use ImageJ to manually circle the cell edges and calculate the area of the CG4 cells. The cell complexity was higher in the control group after differentiation, and the circled areas were more circular. However, the cells contained fewer small branches and the circled images were irregular polygons in the KO group.

Recombinant virus production

Lentivirus production was performed as described previously.[35] Briefly, viral transfer vector DNA and packaging plasmid DNA were transfected into cultured 293T cells using Vigofect. The medium was collected and pooled at 24, 48, and 72 h, and then filtered through a 0.2 μm filter. Viruses were concentrated by ultracentrifuge at 2,0000 rpm for 2 h at 20°C using an SW27 rotor (Beckman). The virus was washed once with phosphate-buffered saline (PBS) and then re-suspended in 150 μL PBS. Lentivirus was stored at −80°C in equal packages, and the subsequent *Trappc12* knockdown test was conducted with the amount just enough to infect almost all OPC.

The shRNA sequences for knockdown Trappc12 are as follows:

shRNA-1: TCGAGTCCCAGATGGTGAAAT
shRNA-2: GCTGCTGTGTGTCTGCTTTAC

Co-IP, western blotting and gray statistics

Co-IP and western blotting were described previously.[22,36] In brief, transfected cells were lysis with special buffer containing 50 mM pH 7.4 Tris-HCl, 100 mM NaCl, 2 mM EDTA and 1% NP-40. Protease inhibitors must be added before use. Cell lysates were centrifuged at 12,000 rpm for 15 min at 4°C. Supernatant were incubated with flag M2 beads 2 h at 4°C. Bound proteins were eluted from beads with 2 × SDS buffer after four to six times washing. Brain tissues from all mice were lysate in RIPA containing 50 mM pH 7.4 Tris-HCl, 150 mM NaCl, 0.5% DOC, 1 mM EDTA and 1% NP-40. Sample lysates were centrifuged at 12,000 rpm for 15 min at 4°C.

The protein concentration was measured by the Bio-Rad method. Prepared samples were subjected to different concentrations of SDS–polyacrylamide gel electrophoresis (SDS–PAGE). All the Western blotting was representative of at least three individual experiments. Expression levels of all proteins were evaluated by gray value with ImageJ, and the average level of relative abundance of each protein in control mice or cells were normalized to 1.

Perfusion and immunostaining analysis

Mice were anesthetized with Ketamine (200 mg/kg) followed by transcardial perfusion with phosphate buffered saline (PBS) and 4% paraformaldehyde. The dissected brains were fixed in 4% paraformaldehyde overnight at 4°C and dehydrated in 30% sucrose, embedded in

optimum cutting temperature compound, and sectioned 30 μm thickness slices. Cultured cells were fixed with 4% PFA at room temperature for 10 min or cold methanol at −20°C for 3 min. The brain slices or cultured cells were first incubated with blocking buffer (10% FBS, 5% BSA, 0.3% Triton X-100, 0.1% NaN_3 dissolved in PBS) at room temperature for 1 h, and then incubated in the primary antibody dissolved in the blocking buffer at 4°C for overnight or 37°C 1 h, and finally incubated in the secondary antibody conjugated with Alexa Fluor 488, 568, or 647 dyes dissolved in the blocking buffer at room temperature for 1 h.

Black gold II staining

For Black gold II staining, brain slices come from the mice for immunofluorescence staining. The procedures are as follows: the brain slices were attached to APES-coated slices and dried overnight at room temperature. Black gold II staining kit was bought from Millipore company. Detailed steps were performed as previously described.[37] Briefly, the brain slices were rehydrated in MilliQ H_2O for 2 min, and then transfer to a 0.3% Black gold II solution preheated to 60°C. Taking out the tissue every 4 min to monitor the tissues until the myelin sheath structure becomes clear, followed by washing with MilliQ H_2O about twice. Next, incubate brain slices with 1% sodium thiosulfate solution at 60°C for 3 min, to remove excess Black gold II dye, and rinsed two times with MilliQ H_2O. Finally, resin seals the stained slices after a series of dehydration and transparency processes.

Transmission electron microscopy (TEM) and statistical analysis

The procedures of TEM were described as previously.[22] Concisely, mice were anesthetized and perfusion with PBS or 0.9% NaCl followed by 2.5% glutaraldehyde and 1% PFA. Corpus callosum was isolated from 1-mm coronal slices and fixed with 2.5% glutaraldehyde, post-fixed in 1% PFA, dehydrated in graded acetone, and then embedded in special resin for TEM. Ultrathin sections must be sagittal sections with thickness of 80 nm. Sections transferred onto copper grids with a carbon film and Images were acquired with a transmission electron microscope (JEM-1400, JEOL, Japan). The number and diameter of myelin sheath was measured by ImageJ software. The g-ratio was calculated as the ratio of axon diameter to myelinated fiber diameter.

BrdU incorporation assay

5-bromo-2′-deoxyuridine (BrdU) was prepared as 100 mg/mL stock solution in sterile saline, aliquoted, and stored at −20°C. Mice were injected intraperitoneally with BrdU 100 mg/kg on the sixth day after birth, then were sacrificed after 24 h. BrdU was exposed to acid treatment as previously described. Next, slices were processed for immunofluorescence analysis using an anti-BrdU antibody.

Electrophysiology and statistical analysis

Brain slice preparation

Mice were anesthetized by isoflurane inhalation and decapitated. The hippocampus was dissected out from the brain and was embedded in low-melting-point agarose. Transverse hippocampal slices were cut at 400 μm thickness using a vibrating slicer in the sucrose-based solution (4°C–6°C) containing the following: 220 mM sucrose, 23 mM $NaHCO_3$, 2.5 mM KCl, 1.25 mM NaH_2PO_4, 0.5 mM $CaCl_2$, 7 mM $MgSO_4$, 1.1 mM sodium ascorbate, 3.1 mM sodium pyruvate and 10 mM glucose. The slices were transferred to and stored in artificial cerebrospinal fluid (ACSF) containing: 119 mM NaCl, 3 mM KCl, 2 mM $CaCl_2$, 1 mM $MgCl_2$, 1.25 mM NaH_2PO_4, 23 mM $NaHCO_3$ and 10 mM glucose at room temperature for at least 30 min before use. All solutions were saturated with 95% O_2 and 5% CO_2.

Field excitatory postsynaptic potentials (fEPSPs) recording

Field excitatory postsynaptic potentials were recorded with a patch-clamp amplifier under infrared-differential interference contrast microscopy. The recordings were made blind to the mouse genotype. Data acquisition and analysis were performed using digitizers and the analysis software pClamp 10. Signals were filtered at 2 kHz and sampled at 10 kHz. Field recordings were made using glass pipettes filled with 1 M NaCl (1–2 MΩ) placed in the stratum radiatum of the CA1 region of the dorsal and ventral hippocampal slices, and fEPSPs were evoked by stimulating the Schaffer collateral pathway at 0.033 Hz with a bipolar tungsten electrode. Input/Output (I/O) curves were generated by plotting the fEPSP slope against the presynaptic fiber volley amplitude following incremental stimulus intensities. The PPF was recorded at an intensity that induced ~40% of the maximal evoked response with 20, 50, 100, 200, and 400 ms inter-pulse intervals. All recordings were performed at 32 ± 1°C by using an automatic temperature controller. The PPF was calculated by dividing the mean amplitude of the second EPSP by that of the first EPSP.

Behavioral assessment and statistical analysis

The number of mice for behavior tests in each group is indicated in the figure legends. All of the procedures were performed as described previously with minor modifications.[36,38]

Open field

Mice were automated locomotion for 1 h in an open field arena (40 cm long × 40 cm wide ×35 cm high). An activity monitoring system (Smart 3.0) was used to track trajectory, followed by quantification of the both moved distance and percent time spent in the margin every 10 min (outside of 20 × 20 cm area).

Rota rod

Beam walking

A modified beam walking test was used to test the balance ability of mice. Briefly, a 1 cm wide and 80 cm long beam was placed about 40 cm above the floor, with one end being a non-transparent box (15 cm long x 15 cm wide x 10 cm high). During the trained phase, mice were placed on one end of the beam and attracted to walk through it. The training lasts for three days, and three times per day before testing. Two cameras are set at the front and back of the beam to record the numbers of foot slides when mice walked through the beam.

Y maze

The equipment of the Y-maze consisted of three white arms at a 120° angle, connected by a central zone. The testing mice should be placed in the test room about 30 min before the experiment begins. Place each testing mouse at the central zone with consistent head orientation each time and allow each mouse to explore freely through the maze during a 10-min session. Mouse behavior was monitored in real time by a video camera with the same system as in the open field test.

Morris water maze

The apparatus of the water maze is a circular pool with a diameter of 120 cm and a depth of 40 cm. a 6 cm diameter platform was hidden in water with white nontoxic paint. The water maze is a relatively simple procedure typically consisting of two phases: acquisition training to find a hidden platform (5 consecutive days and four trials per day). Record the time when mice found the platform during each training. The probe trial was performed on the 6th day. Monitor the time in the target quadrant and the time of passing the original platform area for 1 min after removing the platform from the pool. During both phases, mice should be gently put into the pool, facing the edge of the pool.

Social preference test

The three-chamber apparatus was made of a transparent acrylic box with a removable floor and partitions dividing the box into three equally sized chambers. Age and body weight-matched wild-type male mice were used as stranger mice. Stranger mice must be habituated for 3 consecutive days by placing them inside a 10 cm high inverted wire cage for two independent 30 min every day before the tests. The object is almost equal in volume to the stranger mice. During the habituation phase, two empty inverted wire cups were placed into left and right chambers with both side doors opened, and each test mouse was placed into the middle chamber and allowed to explore for 5 min. In the social preference test stage, the test mouse was gently guided to the middle chamber with both side doors closed. A stranger mouse and object were randomly placed into the left or right inverted wire cage, respectively. After opening the doors connecting the three chambers, the test mouse was allowed to explore for 15 min in three chambers tracked by an activity monitoring system (Smart 3.0). Time spent in each chamber and close interaction with stranger mice or objects were recorded and analyzed.

Ultrasonic vocalization (USV)

Each test 5-month mouse was singly placed in a housing cage at least 3 days before recording courtship USVs. For each recording session, the subject mouse was firstly alone in the recording chamber for 30 min. Subsequently, an ultrasonic microphone (Avisoft Bioacoustics, Berlin, Germany) was placed above. USV emission was recorded by Avisoft e3 Cell Reports 25, 2963–2971.e1–e6, December 11, 2018 Recorder software (Version 4.2) using the following parameters (512 FFT length, 100% frame, Flat Top window and 75% time window overlap) according to the previous report.[39] Recording 5 min as background USVs. To elicit courtship USVs of test male mice, an age-matched strange female mouse was gently placed in the recording container, and USV emission was monitored for 5 min like the recording background. The total number of USVs and call duration were calculated in the automatic parameter analysis for the entire session of 5 min.

QUANTIFICATION AND STATISTICAL ANALYSIS

Statistics

Statistical analyses were performed using GraphPad Prism 9. Data were presented as means ± SEMs. The criteria for significance was *$p < 0.05$; **$p < 0.01$; ***$p < 0.001$; ****$p < 0.0001$. One-way analysis of variance (ANOVA) was used when analyzing the data among WT, cKO, and cKO-Tg, and in the social preference test, and the significance was calculated by Bonferroni correction test; two-way ANOVA was used to analyze the Body weights, brain weight, electrophysiological data, and The significance was calculated by Sidak multiple comparisons test; Data from other assays were analyzed by the unpaired two-tailed t-test.